

Study of Long-Termed Displacements of a Tunnel Boring Machine during its Stoppage

Yanming Yao^a, Nan Lu^{b,*}, Yunming Yang^{b,c}, Yuxuan Cao^c, Hai-Sui Yu^d

^a Ningbo Rail Transit Construction Co. Ltd., Ningbo 315101, PR China

^b Department of Civil engineering, International Doctoral Innovation Centre, University of Nottingham Ningbo China, Ningbo 315100, PR China

^c Ningbo Nottingham New Materials Institute, University of Nottingham Ningbo China, Ningbo 315042, PR China

^d School of Civil engineering, University of Leeds, Leeds LS2 9JT, UK

* Corresponding to: nan.lu@nottingham.edu.cn (Nan LU)

Abstract

This paper studies the long-termed displacement of a tunnel boring machine (TBM) resting on soft clay during its unscheduled stoppage for 100 days. It is based on a real case of tunneling in a coastal city of Ningbo in China. The numerical prediction is carried out by using different soil models in the software PLAXIS, and the prediction is compared with on-site measurement of the displacement. Different factors are considered in the prediction, including soil creeping and the disturbance to the soft clay during the tunneling. The study indicates that the consideration of disturbance is essential to the accurate prediction. While advanced soil models including the soft soil model and soft soil creep model are not able to accurately predict the TBM displacement, the consideration of soil disturbance leads to a very good agreement with the measurement. Accurate predictions of ground settlements also justify consideration of the disturbance in the study of tunneling.

Keywords: Tunnel boring machine (TBM); Long-termed stoppage; Soft clay; Creep; Soil disturbance.

1. Introduction

Modern urban development stimulates the utilization of underground space and underground transport systems. In China, there had been 38 cities with operating metro lines by the end of 2015. In Shanghai alone, 14 metro lines had been constructed within 20 years from 1993 to 2013, reaching the world's longest metro operating mileage of 617 km. Tunneling can encounter various challenges, such as crossing rivers and passing by or even cutting through existing buildings (Bernat and Cambou, 1998; Lee and Nam, 2001; Loganathan et al., 2000; Comodromos et al., 2014). In urban areas, there are strict requirements on ground subsidence due to tunneling in order to minimize its influences on neighboring constructions. Its impacts on deep foundations also need to be investigated. Another important challenge is the poor quality of soil, such as soft clay encountered in tunneling (Loganathan and Poulos, 1998; Shen et al., 2014; Liu et al., 2011). In addition to low strength and low permeability of soft clay, it is characterized with creeping. Consideration of creeping in soft clay is essential in the prediction of long-termed displacement

in geotechnical engineering. Various soft clay models considering creep have been developed and applied with considerable success (Vermeer et al., 1998; Vermeer and Neher, 1999; Borja and Kavazanjian, 1985). The creep model in the soft clay is also employed in the well-established geotechnical engineering software PLAXIS. Numerous studies indicate that the use of creep models in soft clay can improve the accuracy of displacement predictions, especially for long-termed displacements (e.g. Yi et al., 1993; Brinkgreve, 2004). Disturbance of soft clay is another important characteristic in tunneling. The destruction of natural soft clay structure can significantly reduce its strength and stiffness. It is essential to consider the disturbance in tunneling predictions. For example, Mair and Taylor (1997) indicates that consideration of soft clay disturbance has important implications on the study of responses of pile supported buildings due to tunneling. Xu et al. (2003) compares the field measured cone penetration resistance of Shanghai silty clay before and right after the tunneling, and indicates that its shear strength and stiffness are reduced up to half of their original values due to the tunneling disturbance. They also develop the region of disturbance, which takes a shape of waterdrop.

Another important issue in tunneling is unscheduled stoppage of the TBM. The unscheduled stoppage can result from various reasons, such as unexpected failure of power supply, an encounter with unknown soil stratigraphy or deep foundations, and occurrence of incidents. The unscheduled TBM stoppage, especially the long-termed stoppage, can lead to serious problems. For example, Clough et al. (1983) indicates that, in the first earth pressure balance (EPB) shield project in the US, the ground settlement can be as large as 7.6 cm in 5 months in the area below which the TBM stops for 15 days due to a power connection problem. Further study by Rowe and Lee (1994) indicates that the large ground settlement can be attributed to the increased soil volume loss at the tunnel face due to the TBM stoppage. During the stoppage, the face pressure gradually decreases owing to soil consolidation at the bulkhead. In addition, the restart of the TBM from stoppage requires a larger jack force than that used in the normal excavation as a result of the soil consolidation around the shield skin. One significant but ignored issue during the TBM stoppage is the displacement of the TBM itself. Without proper controls during the long-termed stoppage, large weight of the TBM resting on soft clay can lead to considerable settlements. In addition, unevenly distributed weight of the TBM can also lead to tilting of the TBM. Inappropriate TBM face supporting pressures during the stoppage can accelerate its displacements or make its surrounding soil fail. All the issues can also make its restart difficult or damage the TBM.

The work presented here is motivated by a successful long-termed stoppage of the TBM in tunneling in the city of Ningbo, a portal city in East China, and a large part of ground contains soft clay. The TBM stopped for 100 days, and the TBM displacement and the ground settlement were monitored and properly controlled. This paper aims to compare numerical simulations with field measured displacements of the TBM and the ground surface. Since the study of the TBM displacement is usually neglected, the priority is given to it. The numerical model considers impacts of different factors, including the creeping and soil disturbance. The well-established geotechnical engineering software PLAXIS is used. It has been proven effective in numerous studies of tunneling (Vermeer et al., 2002; Klar et al., 2007; Chehade and Shahrour, 2008; Ng et al., 2016).

2. Engineering Background

The Ningbo metro line 3, with a length of 25.7 km, is a north-south oriented metro line and passes through the central region of the city. The excavation is carried out with an EPB type of TBM, which is 9155 mm long, and 6340 mm in diameter at its face. The TBM weighs 338 tons, and its center of gravity is at approximately one third of the length from its face. The tunnel face is stabilized by the pressure of the excavated soil itself. The TBM is pushed forward by hydraulic jacks behind its tail, and the cutting head excavates soil and moves forward at a speed of 3~5 cm/min. Prefabricated reinforced concrete lining rings are bolted together at the back of the TBM. The lining ring is 1200 mm in length, 6200 mm in external diameter and 350 mm in thickness. The bulk density of reinforced concrete is 35 kN/m³. During construction of the section between Datong bridge station and Zhongxing bridge station in metro line 3, there was an unscheduled long-termed stoppage of the TBM. The machine was shut down on the 19th of March 2016, and the excavation was paused until the 27th of June 2016, which means the TBM stoppage lasted for 100 days. The alignment of the tunnel route near the location of stoppage is shown in Figure 1. The figure shows that there are many constructions on the ground surface, which imposes strict requirements for allowable ground surface settlement. The lining rings are assigned numbers in the figure, and one digit represents the length of a ring of 1200mm.

The TBM was shut down after the 371st lining ring was installed. The jack force was applied at the tail of the TBM during the stoppage. There were in total 22 hydraulic jacks, located in four zones along the perimeter of the concrete lining, including the top having 6 jacks, the bottom having 6 jacks and the two side zones having 5 jacks each. Although the jack readings during stoppage period cannot be monitored, these jack forces were carefully adjusted according to the face supporting pressure generated at the TBM face. The face pressure was monitored by the left and right pressuremeters placed at the axis level on the TBM face. The average face pressure during 100 days of stoppage is about 360 kPa, which is larger than the initial static lateral total earth pressure of 280 kPa. At the ring directly behind the TBM, grouting was injected into the tunnel soil to provide a temporary support. The grouting pressure increases linearly with depth by a gradient of 20 kPa/m, and the average value at the tunnel axis was estimated as 360 kPa from the pressured in the jetting pipe. There were back-up trailers resting inside the constructed tunnel, and the total weight was 106 tons. They can be represented by sets of twin point loads, and their distribution is shown in Figure 2.

The soil stratigraphy in this region is shown in Figure 3. The ground water table is 1 m below the ground surface. The soil stratigraphy comprises a fill layer, four clay layers and two silt layers. When the TBM stoppage happens, the entire TBM is in ④2 clay layer. The physical and mechanical properties of these soils are given in Table 1. They are obtained from laboratory tests of soil specimens taken from the construction site. Among them, the strength, loading history and compression parameters at some locations for ③1 silt and ⑥2T silt are obtained from test results of similar soils in an adjacent site. The soil parameters in the fill layer are not available and typical values are assumed. The laboratory measured coefficient of permeability for the clay is very small, and 1.0×10^{-7} cm/s and 1.5×10^{-7} cm/s are recommended to be used in designs along

vertical and horizontal directions, respectively. The silt layers are far from the tunnel, and it is also recommended to use the same values. Table 1 shows that the soils are generally very soft, characterized with high water contents, high void ratios, medium to high compressibility, low permeability and normal or slight consolidation.

The displacement of the TBM face and tail was closely monitored at its axis **by the built-in instrument of the TBM, and its data was recorded daily.** Figure 4 presents the measured data, in which a negative value denotes the settlement and a positive value denotes the rise. It is seen that the TBM face moved down and stabilized at 9 mm, while its tail moved up and stabilized at 6 mm. The difference in displacements is the result of uneven weight distribution of the TBM, as its gravity center is located at one third of its length to its face. Therefore, the front soil is subjected to a larger pressure than the back soil. Since the TBM can be approximated as a rigid body, it tilts due to the different displacement at its face and tail.

The ground settlement above the tunnel was also monitored **by leveling instruments installed according to the lining ring numbers shown in Figure 1. Three typical locations are selected and presented here.** They are on the ground above Ring 380 closer to the TBM face, above Ring 370 closer to the TBM tail, and above Ring 360 behind the TBM tail. These ring numbers are put in red boxes in Figure 1, and they are also marked in Figure 3 by dashed arrows. The measured settlements at these three locations are also shown in Figure 4. It indicates that the ground above the TBM face (Ring 380) experiences the smallest settlement of 3 mm, and the ground settlement above the TBM tail (Ring 370) and behind it (Ring 360) are much larger, at approximately 10 mm. The different ground settlement is understandable since the tunnel in front of the TBM face has not been excavated.

3. Numerical Simulations

3.1. Finite element model

The numerical analysis is carried out by using the finite element software PLAXIS 3D 2017. For the sake of simplicity, the numerical model simulates a greenfield condition, in which the influences of constructions on and below the ground surface are ignored. Due to the symmetry of the problem, only half of the domain is considered. The finite element model is shown in Figure 5. The whole model is 50 m in width, 80 m in length and 40 m in depth. The tunnel axis is located at the depth of 20 m. The TBM stops at 41.6m. 10-node tetrahedral elements are used, and there are in total 18190 elements and 27257 nodes in the model. The TBM made from steel can be approximated as a rigid body. It is 9200 mm long and takes a conical shape with the external diameter varied from 6340 mm at the face to 6200 mm at the tail. To consider its unevenly distributed weight, the TBM is split into two parts to add weight, shown in Figure 5. Its first part at the front is one third of the TBM length and carries two thirds of its weight. The second part at the back is two thirds of the TBM length and carries one third of its weight. **Consequently, the total center of gravity of the TBM is located at one third of its length to its face, as in the real engineering condition.** Other model substances, including the tunnel face pressure, grouting pressure, weight and dimension of the concrete lining, weight of the TBM and

back-up trailers, and the ground water level are all applied the same as in on-site conditions.

The process to simulate the tunnel construction and following consolidation starts with the calculation of the initial stress field from soil self-weight in the first phase. The densities and initial lateral stress pressure coefficients for different soils are given in Table 1. In the second phase of simulation, the TBM is advanced to its stoppage location at 41.6 m. In this phase, the structural plate elements are used for the TBM and lining, in order to facilitate the application of the volume loss due to the varied diameter of the TBM along its length. Meanwhile, the tunnel face support pressure, grouting pressure, weights of the TBM, and the interface between the structural elements and adjacent soil are activated. In the third phase, solid elements are used for the TBM, and the concrete lining is activated. The tunnel face pressure is applied through the jack force behind the TBM tail. The point loads representing the trailer weight are also activated. The consolidation is activated in the fourth phase, and it lasts for 100 days.

The soil constitutive model is the key to the finite element simulation. There are plenty of built-in models in PLAXIS, including the Mohr-Coulomb model, soft soil model and soft soil creep model. For detailed descriptions, one can refer to its manual (PLAXIS, 2016). The soft soil model is suitable for normally consolidated or slightly overconsolidated, highly compressible clay and silt. Given the characteristics of soils in the project, the soft soil model is chosen to model soil behaviors in the first step. Besides, the creeping feature can be added on the basis of the soft soil model, which will be discussed in the sequel. The soft soil model consists of an isotropic non-linear pressure dependent elastic relationship, a non-associated perfectly plastic Mohr-Coulomb failure surface, and an associated volumetric hardening yield cap of elliptical shape. The elastic parameters can be represented with C_s in the laboratory experiment. The Mohr-Coulomb failure surface is represented by a friction angle and cohesion. Its dilatancy angle is assumed to be zero. The elliptical yield cap is similar to the Cam-Clay cap, and its parameters can be automatically obtained from C_c in the software. In addition, the soil in the fill layer is modeled by using Mohr-Coulomb model, and typical model parameters are assumed. All the model parameters are shown in Table 1.

Creeping is essential in simulating long-termed behavior of soft clay. The soft soil creep model is also considered for the clayey soil in this project. The model was developed by Vermeer et al. (1998) on the basis of the soft soil model in the software. It is similar to the soft soil model on the aspects of elasticity, Mohr-Coulomb failure surface, elliptical plastic potential and compression index. It assumes that all inelastic strain is time-dependent, and the creep volumetric stain in one dimension is defined as,

$$\dot{\varepsilon}_v^c = \frac{\mu^*}{\tau} \left(\frac{1}{OCR_p} \right)^{\frac{\lambda^* - \kappa^*}{\mu^*}} \quad \text{Eq (1)}$$

Where τ denotes a constant period of time, which is one day in PLAXIS. OCR_p is the over-consolidation ratio. λ^* and κ^* are compression parameters used by the model for the plastic and elastic loading, respectively. They can easily be related to the more widely used compression and swelling indices C_c and C_s . μ^* is the model parameter for the creep mechanism, which is usually obtained from an oedometer test. For practical reason, the creep parameter can also be obtained from the relationship $\mu^*/\lambda^*=k$, where k is a constant for a given soil (Mesri and

Godlewski, 1977). Laboratory experimental results in the project indicate that the average value of k is 0.0335 for the Ningbo soft clay. This value is within the range of $k=0.04\pm 0.01$ for inorganic clays given by Mesri and Godlewski (1977) and is adopted in this paper.

3.2. Numerical Results

The on-site measured displacements and simulation results at the TBM face and tail by using the soft soil model are shown in Figure 6. The predicted displacements increase over time and tend to stabilize due to consolidation. The TBM face goes down and the tail goes up. The rotation occurs because the TBM weight is unevenly distributed, and its gravity center is approximately at one third of its length to the TBM face. The soil near the TBM face undergoes loading while the soil near the tail undergoes unloading, compared to their original stress states before the excavation. It should be noted that the displacements of the TBM face and tail are complex. They influence each other because the TBM is approximately a rigid body. The face displacement is more dominant because the gravity center is closer to the face. Although the overall trend of the calculated displacements is the same as that from the measured displacements, with the face going down and tail up, their displacement magnitudes are different. It is especially true for the face displacement of 9 mm in the measurement and 0.5 mm in the computation. In addition, the calculated rise of 4 mm at the tail is much larger than the calculated settlement of 0.5 mm at the face, which gives an average rise for the whole TBM. This is because the weight of the excavated soil is larger than the weight of the TBM. In reality, the measured average displacement for the whole TBM goes down with the settlement at the face larger than the rise at the tail, as discussed after Figure 4.

The soft soil creep model is used next. Its prediction is also shown in Figure 6 to compare with the results by using the soft soil model and measurements. The figure indicates that the consideration of creep enables the TBM face settlement larger than that according to the soft soil model. The TBM tail rise is also slightly reduced, and the reduced rise is much smaller than the increased settlement. This is because the creep creates an additional plastic strain. In addition, as the soil pressure near the TBM face is larger than its original pressure before the excavation, the value of OCR_p is one. In contrast, the soil pressure near the tail is smaller than its original pressure, and the value of OCR_p is larger than one. Equation (1) indicates that a smaller OCR_p leads to a larger creeping impact. Therefore, the increase of TBM face settlement is dominant over the reduction of the TBM tail rise as a result of considering the creep. Figure 6 shows that, although the predicted face settlement considering the creep is much larger than that excluding creep, it is still far from the measured settlement.

3.3. Disturbance Impact

It is well established that the soft clay structure can be damaged during the excavation, and its strength and stiffness are reduced by the disturbance. Xu et al. (2003) carried out an in-depth study by measuring soil property at many different locations surrounding an excavated tunnel before and after the excavation in the city of Shanghai by using cone penetration and vane shear tests. They indicated that the soil strength and stiffness could be reduced as large as half by the

disturbance. They also estimated the range of disturbance after tunneling, which takes a shape of pear or waterdrop. It is shown in Figure 7, in which the horizontal span of the disturbance region at the tunnel middle is approximately 60% of the tunnel radius. The city of Ningbo, where the current project was conducted, is only 200 km from the city of Shanghai, and they are both coastal cities in the estuary region of the Yangtze River. Their soil properties are also similar. In the current study, a circular shape of disturbance region instead of pear is used. **This simplification enables an easier model set-up including the specification of soil disturbance.** Similar approximation has been used in an earlier study by Yi et al. (1993). Thus, a hollow cylinder of disturbance region surrounds the tunnel, and its boundary is at half of the tunnel diameter from the tunnel. In front of the tunnel face, there is a semi-sphere of disturbance region enclosing the hollow cylinder. They are shown in Figure 8.

It is assumed that the strength and stiffness of the disturbed soil is reduced by a factor of reduction (FOR). The $\tan\phi'$ controlling the strength is reduced by FOR. The C_s controlling the elastic stiffness is increased by FOR because the elastic response is also important in the tunnel excavation as it involves unloading and reloading. The C_c directly controlling the plastic stiffness remains unchanged. It is because the change of C_c is complex, which also strongly influences the creeping, as shown in the creeping equation. Nevertheless, the plastic stiffness has been indirectly reduced by the reduction of friction angle. The hollow cylinder and semi-sphere of disturbed region covers the entire ④ 2 clay layer and parts of ③ 2 and ⑥ 2 silty clay layers, and the reduction applies to all the influenced soils.

Different values of FOR are considered, including 0.3, 0.5 and 0.6. Figure 9 shows their predictions using the soft soil creep model compared to the measurements. It indicates that the FOR has a considerable impact on the predicted displacement, and it markedly increases the displacement for both TBM face and tail. A larger reduction leads to a larger settlement. Compared to much smaller TBM face displacements than the measurement in previous predictions without the disturbance, the FOR of 0.6 even brings the displacement larger than the measurement. In addition, the impact of FOR is greater on the TBM face than the TBM tail. It is because the soil near the TBM face is subjected to an increased loading as a larger part of the TBM weight is at the front, and the reduced friction angle brings the stress closer to the failure. Thus, a larger FOR makes the average displacement of the entire TBM go down, instead of the rise in previous predictions without the disturbance. Figure 9 also shows that the value of FOR=0.5 gives a very good agreement between the prediction and the measurement for both the face and tail displacements.

All the above simulations are for the tunnel face pressure of 360 kPa, which is the on-site pressure. Impacts of different tunnel face pressures are also studied. Figure 10 shows the predicted TBM face and tail displacements after 100 days of stoppage by using various face pressures. It indicates that both the too small and the too large face pressures lead to large displacements. The leftmost prediction corresponds to no jack force and the face pressure is only associated with the friction between the TBM and surrounding soil. The TBM face settlement can be as large as 20 mm in this extreme case. This is because the soil in front of the TBM starts yielding under a small supporting face pressure, and it influences the soil underneath the TBM

face. The middle range of face pressures gives the smallest displacements, and the on-site face pressure of 360 kPa is among it. When the face pressure becomes too large, the soil in front of the TBM is subject to a large horizontal pressure leading to soil yielding, which also influences the soil underneath the TBM face. In fact, the horizontal displacement of the TBM becomes very large as well in this case.

The ground settlements are also predicted at the locations above the TBM face (Ring 380), the TBM tail (Ring 370), and behind the TBM tail (Ring 360), respectively, as shown in Figure 3. Similar to the study of the TBM displacement, the predictions use the soft soil model, the soft soil creep model and the soft soil creep model considering the disturbance. The predictions together with the on-site measured settlements are shown in Figure 11. It indicates that the soft soil model gives the smallest settlements, which are much smaller than the measurements. The use of the soft soil creep model improves the predictions and the further consideration of the disturbance gives the best agreement with the measurements. The largest predicted settlement is 7.3 mm, which agrees well with the largest measured settlement of approximately 10 mm. In addition, the trends of the predicted displacements are also consistent with those for the measurements. The displacements on the ground above the TBM tail and behind the TBM tail are close to each other and larger than that above the TBM face. This is because the tunnel in front of the TBM face has not been excavated, as discussed before. In summary, the good agreement between the predictions and measurements in ground settlements also justifies the consideration of the disturbance.

4. Conclusion

This paper analyzes the displacement of a TBM during its unscheduled long-termed stoppage. The study is based on a real case of tunneling in the city of Ningbo in China. The tunneling takes place in soft clay. Its displacement pattern is complex as the TBM weight is not evenly distributed, resulting in the settlement at its front and the rise at its tail. The finite element analysis is carried out using the software PLAXIS and the numerical predictions of the TBM displacement are compared with on-site measurements. Both the soft soil model and the soft soil creep model are used in the numerical simulations. Their predictions are in poor agreement with the measurements in both the displacement pattern and magnitudes. To improve the prediction, the disturbance to soft clay is considered during the tunneling. A hollow cylindrical disturbance zone enclosed by a semi-sphere is assumed and the soil strength and stiffness are reduced to various levels. The prediction considering the disturbance is in very good agreement with the measurements. The ground settlement is also predicted by using these models with and without the disturbance impact. Similarly, the prediction of the ground settlement considering the disturbance agrees very well with the measurement, which is much better than the predictions without the disturbance.

Acknowledgements

The authors acknowledge the financial support from the International Doctoral Innovation

Centre, Ningbo Education Bureau, Ningbo Science and Technology Bureau, and the University of Nottingham. This work was also supported by the UK Engineering and Physical Sciences Research Council (Grant No. EP/G037345/1 and EP/L016362/1), NSFC (Project code 11872219), and the National Basic Research Program of China (Grant No. 2014CB047006). These supports are appreciated.

References

- Bernat, S., Cambou, B., 1998. Soil-structure interaction in shield tunnelling in soft soil. *Computers and Geotechnics*. 22, 221-242.
- Borja, R., Kavazanjian, E., 1985. A constitutive model for the stress-strain-time behaviour of 'wet' clays. *Geotechnique*, 35, 283-298.
- Brinkgreve, R., 2004. Time-dependent behaviour of soft soils during embankment construction—a numerical study. *Proc. NUMOG IX*. 631-637.
- Cehade, F. H., Shahrou, I., 2008. Numerical analysis of the interaction between twin-tunnels: Influence of the relative position and construction procedure. *Tunnelling and Underground Space Technology*. 23, 210-214.
- Clough, G. W., Sweeney, B. P., Finn, R. J., 1983. Measured soil response to EPB shield tunneling. *Journal of Geotechnical Engineering*. 109, 131-149.
- Comodromos, E.M., Papadopoulou, M.C., Konstantinidis, G.K., 2014. Numerical assessment of subsidence and adjacent building movements induced by TBM-EPB tunneling. *Journal of Geotechnical and Geoenvironmental Engineering*, 140, 04014061.
- Klar, A., Vorster, T., Soga, K., Mair, R., 2007. Elastoplastic solution for soil-pipe-tunnel interaction. *Journal of Geotechnical and Geoenvironmental Engineering*. 133, 782-792.
- Lee, I.M., Nam, S.W., 2001. The study of seepage forces acting on the tunnel lining and tunnel face in shallow tunnels. *Tunnelling and Underground Space Technology*. 16, 31-40.
- Liu, G.B., Jiang, R.J., Ng, C.W.W., Hong, Y., 2011. Deformation characteristics of a 38 m deep excavation in soft clay. *Canadian Geotechnical Journal*. 48, 1817-1828.
- Loganathan, N., Poulos, H., 1998. Analytical prediction for tunneling-induced ground movements in clays. *Journal of Geotechnical and geoenvironmental engineering*. 124, 846-856.
- Loganathan, N., Poulos, H., Stewart, D., 2000. Centrifuge model testing of tunnelling-induced ground and pile deformations. *Geotechnique*. 50, 283-294.
- Mair, R., Taylor, R., 1997. Theme lecture: Bored tunneling in the urban environment. *Proceedings of the 14th international conference on soil mechanics and foundation engineering, Hamburg, Balkema, Rotterdam, The Netherlands*. 4, 2353-2385.
- Mesri, G., Godlewski, P. M., 1977. Time and Stress-Compressibility Interrelationship. *Journal of the Geotechnical Engineering Division*. 103, 417-430.
- Ng, C.W.W., Wang, R., Boonyarak, T., 2016. A comparative study of the different responses of circular and horseshoe-shaped tunnels to an advancing tunnel underneath. *Geotechnique Letters*, 6, 168-175.
- PLAXIS, 2016. *PLAXIS 3D Material Models Manual*. PLAXIS BV, Delft, Netherlands. [Online] Available at: <https://www.plaxis.com/support/manuals/plaxis-3d-manuals/> <Accessed on 12/23/2017>

- Rowe, R.K., Lee, K.M., 1994. Subsidence owing to tunnelling. II. Evaluation of a prediction technique: Reply. *Canadian Geotechnical Journal*. 31, 467-469.
- Shen, S.L., Wu, H.N., Cui, Y.J., Yin, Z.Y., 2014. Long-term settlement behaviour of metro tunnels in the soft deposits of Shanghai. *Tunnelling and Underground Space Technology*, 40, 309-323.
- Vermeer, P., Neher, H., 1999. A soft soil model that accounts for creep. Proceedings of the international symposium Beyond 2000 in Computational Geotechnics, Balkema, Rotterdam, The Netherlands. 249-261.
- Vermeer, P., Stolle, D., Bonnier, P., 1998. From the classical theory of secondary compression to modern creep analysis. Proc. 9th Int. Conf. Computer Methods and advances in Geomechanics, Wuhan, China. 2469-2478.
- Vermeer, P., Ruse, N., Marcher, T., 2002. Tunnel heading stability in drained ground. *Felsbau*. 20, 8-18.
- Xu, Y., Sun, D.A., Sun, J., Fu, D., Dong, P., 2003. Soil disturbance of Shanghai silty clay during EPB tunnelling. *Tunnelling and underground space technology*. 18, 537-545.
- Yi, X., Rowe, R.K., Lee, K.M., 1993. Observed and calculated pore pressures and deformations induced by an earth balance shield. *Canadian Geotechnical Journal*. 30, 476-490.

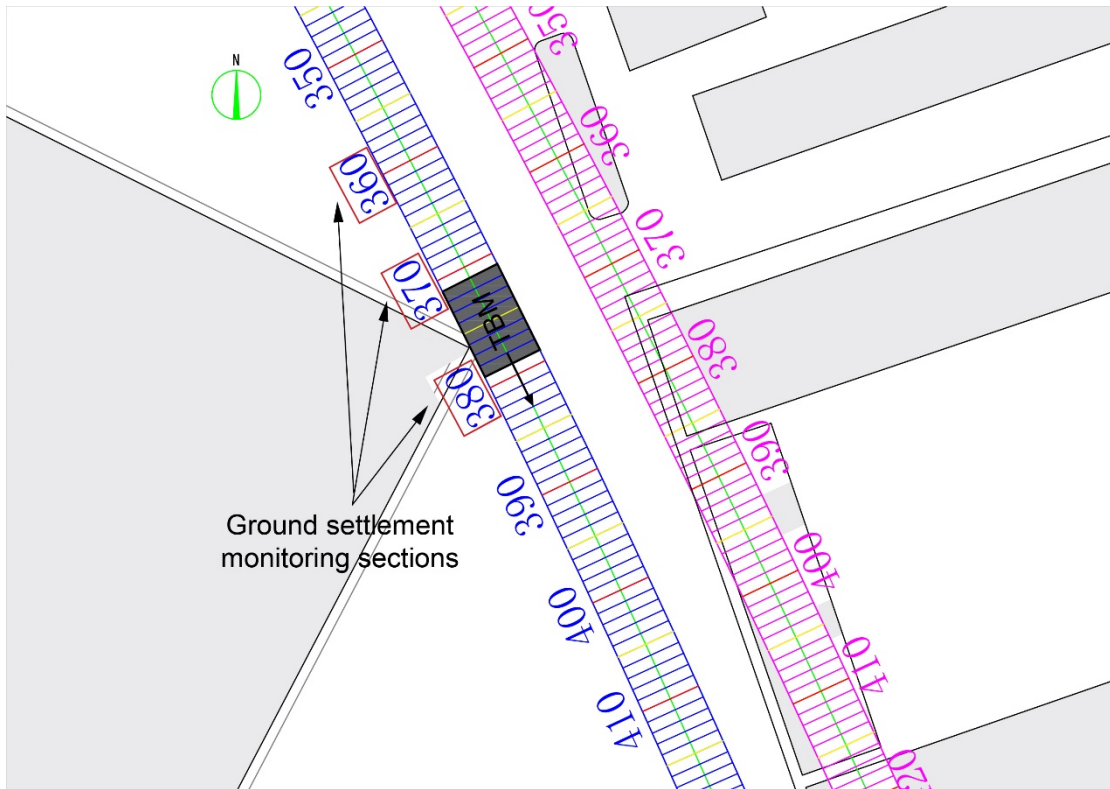


Figure 1. Plane view of the tunnel alignment and locations for TBM stoppage and ground monitoring

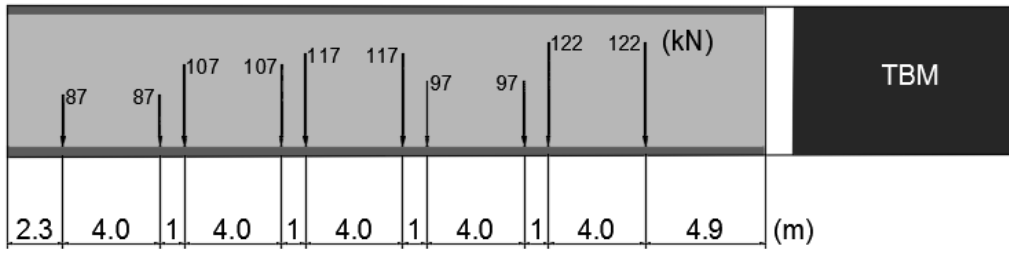


Figure 2. Distribution of point loads that represent back-up trailer weights

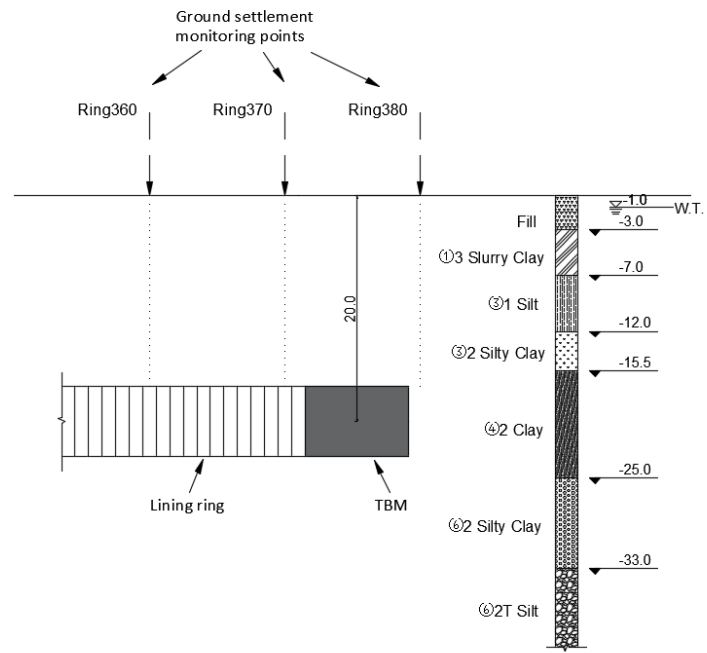


Figure 3. Cross sectional view of the soil stratigraphy at the site of TBM stoppage

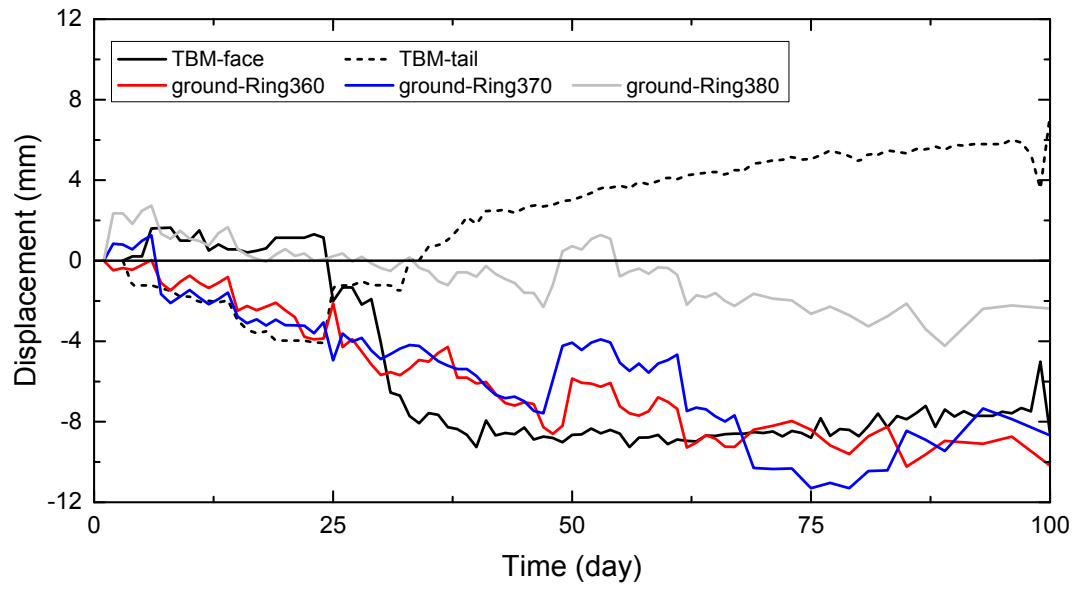


Figure 4. Field measured TBM displacement and ground settlement during the stoppage

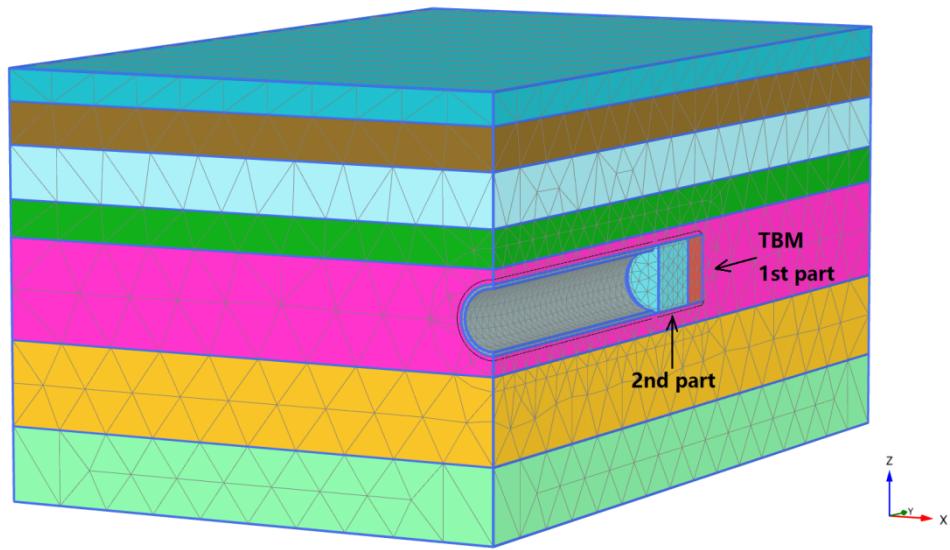


Figure 5. Finite element mesh for the TBM stoppage problem

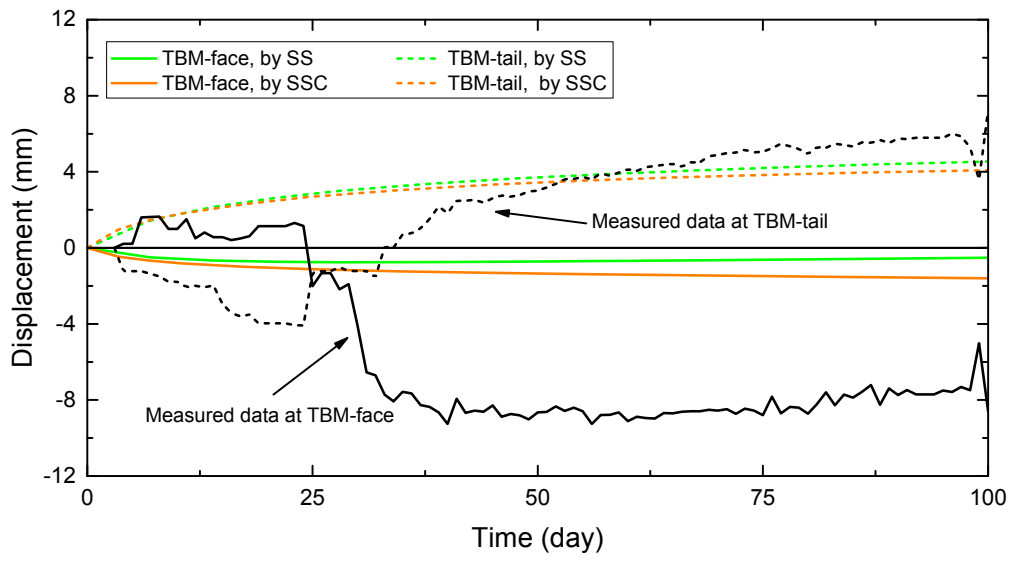


Figure 6. Measured and predicted TBM displacements at its face and tail with the soft soil (SS) model and soft soil creep (SSC) model

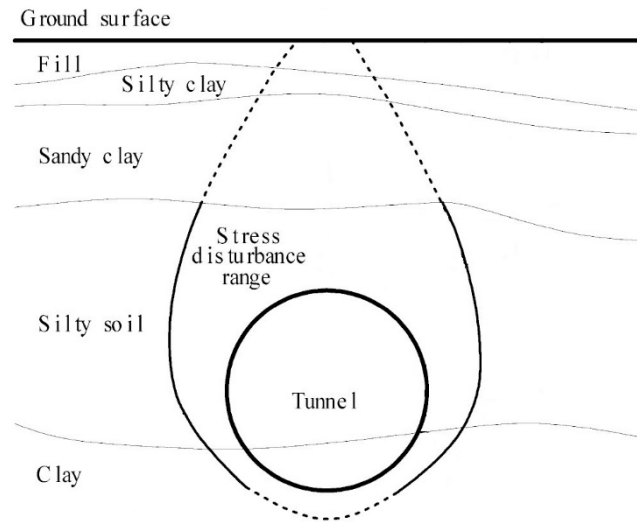


Figure 7. Disturbance region after tunneling estimated by Xu et al. (2003)

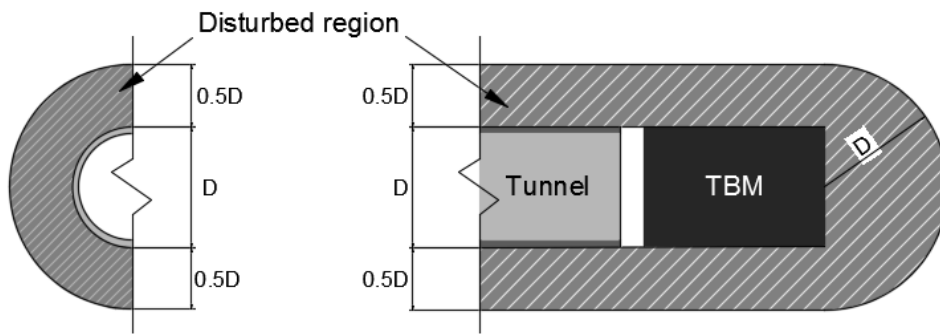


Figure 8. Schematic diagram of disturbed region in the simulation

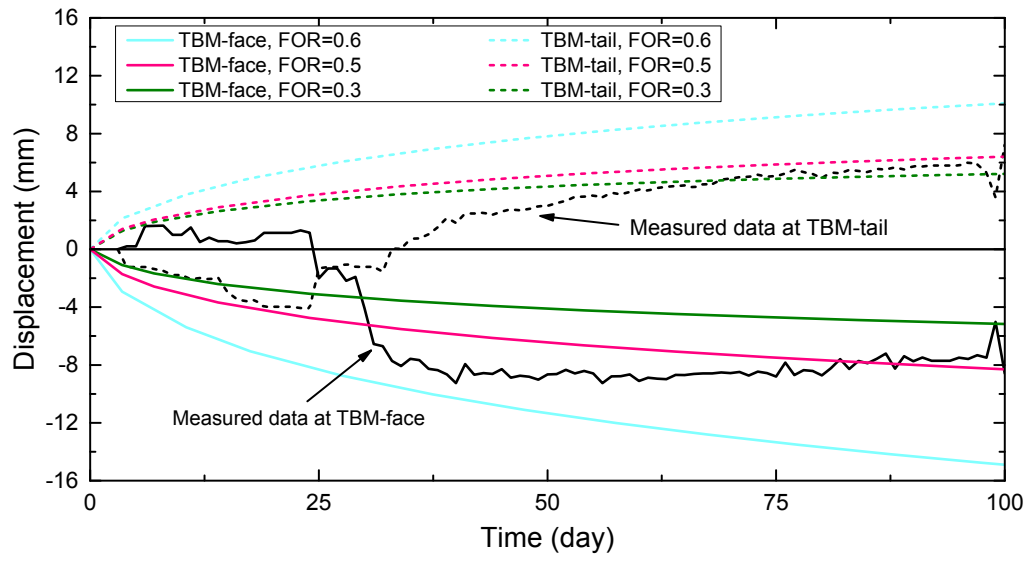


Figure 9. Measured and predicted TBM displacements at its face and tail with the soft soil creep (SSC) model by considering the soil disturbance

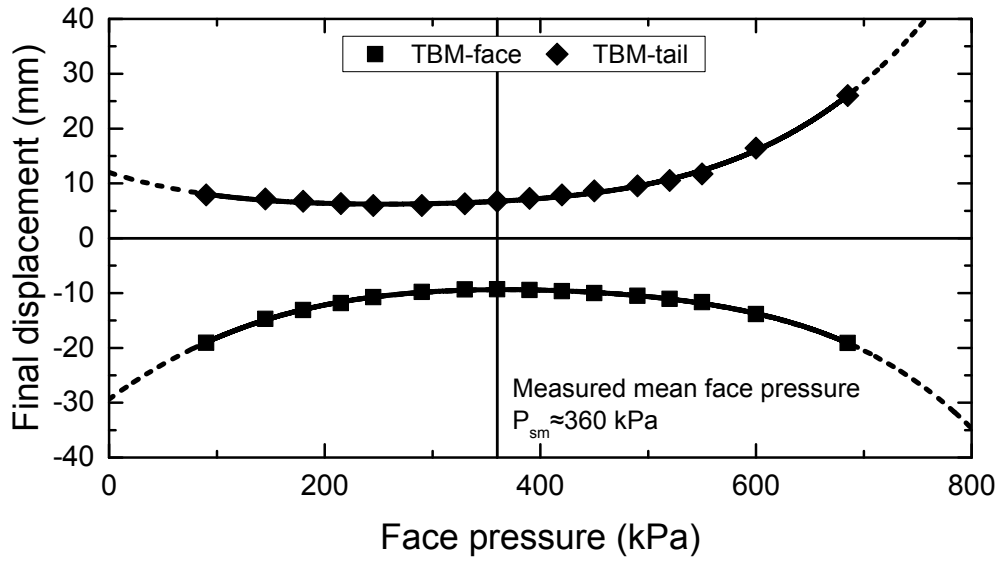


Figure 10. Predicted TBM final displacements at its face and tail after 100 days under various face pressures

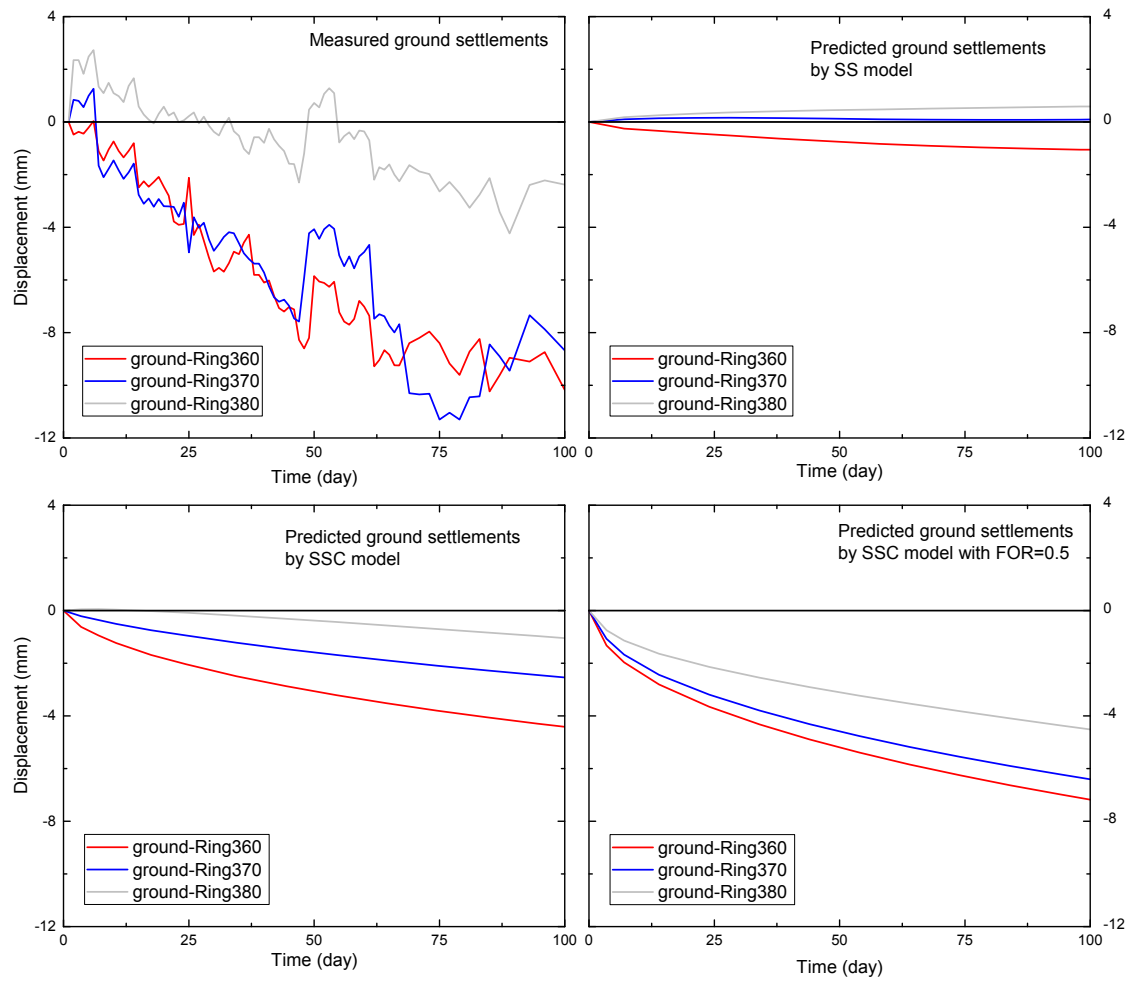


Figure 11. Measured and predicted ground settlements at different locations (Ring360 behind TBM tail; Ring370 above TBM tail; Ring380 above TBM face)

Table 1. Physical and mechanical properties of soils at the tunnel stoppage site.

| Layer | | Fill | ① 3 slurry clay | ③ 1 silt | ③ 2 silty clay | ④ 2 clay | ⑥ 2 silty clay | ⑥ 2T silt |
|---|----------------|---------|-----------------|----------|----------------|-----------|----------------|-----------|
| Constitutive model | | MC | SS or SSC | SS | SS or SSC | SS or SSC | SS or SSC | SS |
| Bulk density (kN/m ³) | γ_{sat} | 20 | 17.29 | 18.96 | 18.69 | 17.69 | 18.64 | 18.67 |
| Water contents (%) | w | - | 48.05 | 26.24 | 28.96 | 40.61 | 29.75 | 26.38 |
| Liquid limit (%) | w_L | - | 42.69 | 28.11 | 29.79 | 42.92 | 32.81 | - |
| Plastic limit (%) | w_p | - | 23.38 | 20.32 | 17.78 | 22.98 | 19.75 | - |
| Initial void ratio | e_{init} | default | 1.268 | 0.764 | 0.868 | 1.121 | 0.888 | 0.844 |
| Young's modulus (kPa) | E' | 10000 | - | - | - | - | - | - |
| Poisson ratio | ν' | 0.2 | - | - | - | - | - | - |
| Effective cohesion (kN/m ²) | c'_{ref} | 4 | 7.7 | 4 | 12 | 6.5 | 13 | 4 |
| Effective friction angle (°) | ϕ' | 10 | 25.9 | 34 | 28.4 | 25.1 | 29.3 | 35 |
| Compression index | C_c | - | 0.375 | 0.174 | 0.187 | 0.404 | 0.186 | 0.166 |
| Swelling index | C_s | - | 0.057 | 0.016 | 0.021 | 0.06 | 0.02 | 0.017 |
| Pre-consolidation pressure (kPa) | P_p' | - | 50.4 | 91.2 | 161.3 | 218.3 | 423.3 | 424.3 |
| Static lateral stress coefficient | K_0 | - | 0.57 | 0.44 | 0.44 | 0.52 | 0.43 | 0.36 |